5-2016

Efficient 3D dental identification via signed feature histogram and learning keypoint detection

Zhiyuan ZHANG
Singapore Management University, zhiyuanzhang@smu.edu.sg

Sim Heng ONG

Xin ZHONG

Kelvin W. C. FOONG

Pattern Recognition 60 (2016) 189–204

Contents lists available at ScienceDirect

Pattern Recognition

journal homepage: www.elsevier.com/locate/pr

Efficient 3D dental identification via signed feature histogram and learning keypoint detection

Zhiyuan Zhang [a,b], Sim Heng Ong [c], Xin Zhong [d], Kelvin W.C. Foong [a,*]

[a] Faculty of Dentistry, National University of Singapore, 11 Lower Kent Ridge Road, Singapore 119083, Singapore
[b] Research and Technology, Lenovo, Shenzhen 518067, China
[c] Faculty of Engineering, National University of Singapore, Singapore 117583, Singapore
[d] Institute of High Performance Computing, A*STAR, Singapore 138632, Singapore

ARTICLE INFO

Article history:
Received 29 October 2014
Received in revised form
11 September 2015
Accepted 10 May 2016
Available online 24 May 2016

Keywords:
Dental biometrics
Tooth recognition
Postmortem identification
Shape descriptor
Keypoint detection
Shape matching
Random Forest

ABSTRACT

Current methods of dental identification are mainly based on 2D dental radiographs which suffer from speed and accuracy limitations. In this paper, we present an efficient dental identification approach based on 3D dental models. We propose a novel shape descriptor, the Signed Feature Histogram (SFH), which is highly discriminative and can be easily computed to describe the local surface. Based on the SFH, a learning keypoint detection method is adopted to accurately detect the desired keypoints on both antemortem (AM) and postmortem (PM) models. For a given PM model, the optimal initial alignment to the AM model to be matched can be found efficiently and robustly by matching the SFHs between the keypoints. The final matching score is obtained by running the iterative closest point algorithm which further refines the initial alignment. We have performed comparative experiments for the SFH on a public dataset, and state-of-the-art performance is achieved. We also test the identification method on a database of 200 AM models and tested the performance of the proposed approach on 3 different PM datasets comprising complete, incomplete and single tooth models respectively. The experimental results show that both high accuracy and efficiency are achieved with 100% Rank-1 identification accuracy on both complete and incomplete PM models and 74% Rank-1 accuracy on single tooth PM models. The running time is only 300 s on average which is about 80 times faster than many 2D methods which can take several hours to identify one subject.

1. Introduction

Dental identification has emerged as a new biometric strategy and received substantial attention in recent years [1–9]. Compared to other identifiers such as face, fingerprint and palm print, the dental record is regarded as the most promising trait for human identification in the unfortunate and tragic events of homicide and mass disasters as it is the hardest and the most indestructible part of human body [10]. In the mass disasters like 9/11 terrorist attack and the Asian tsunami of 2004, dental identification has shown to be more reliable and effective than other means [11,12]. It even outperforms DNA identification as about 75% of the victims were identified using dental records while DNA only helped identify 0.5% victims in the case of the Asian tsunami [13].

Most existing dental identification approaches rely on 2D radiographs. Radiographs taken before death are stored in an antemortem (AM) database, while a radiograph obtained after death is saved as a postmortem (PM) image which will be used to match against the AM database [14]. Traditional dental identification usually requires forensic odontologists to manually search the AM database and find the best match to the given PM image based on distinctive features such as missing teeth, crown and root morphology, pathology and dental restorations [15]. Since such a manual process is less accurate and time-consuming, automatic or semiautomatic approaches have been developed over the past few years. Jain et al. [1] introduced a semiautomatic dental identification method which requires manual selection of region of interest (ROI). The tooth contours are then extracted and the identification result is obtained by matching the PM and AM tooth contours. To make it more efficient, Jain and Chen [2] proposed a segmentation algorithm to detect ROI and a probabilistic method to automatically find the contours of teeth. However, human intervention is still needed to initialize certain algorithmic parameters and correct errors for poor quality images. While these two semiautomatic methods [1,2] were shown to be feasible on a small database, they performed poorly for blurred images or partially occluded query shapes. In [5], Nomir and Abdel-Mottaleb

* Corresponding author.
E-mail addresses: cszyzhang@gmail.com (Z. Zhang), eleongsh@nus.edu.sg (S.H. Ong), andreayoung123@gmail.com (X. Zhong), kelvinfoong@nuhs.edu.sg (K.W.C. Foong).

http://dx.doi.org/10.1016/j.patcog.2016.05.007
0031-3203/

presented an automatic tooth segmentation technique based on iterative and adaptive thresholding. Signature vectors are used to describe the extracted teeth contours, and the similarities of the AM and PM tooth contours are obtained by matching the signatures. In their later work, they showed that the accuracy and speed can be further improved through a hierarchical contour matching algorithm [16] or a fusion scheme [17].

Despite the popularity of using contours for dental identification, poor image quality often plagues accurate tooth contour extraction and makes the identification unreliable. This has led to the use of more features to improve the robustness. For instance, Nomir and Abdel-Mottaleb [6] showed that the accuracy could be improved by using both tooth contours and tooth appearance which are represented by Fourier descriptors and forcefield energy respectively. Dental works such as crowns, bridges, and fillings which appear as bright regions and are more distinct than teeth can also be used for identification [3,7]. Chen and Jain [3] presented a dental identification system based on matching tooth contours and regions of dental work. Tooth contours are matched using a shape registration strategy while dental work is matched on overlapping areas using an area-based metric. The matching accuracy was improved by fusing these two measurements. Lin et al. [7] proposed to use both contours of teeth and dental works for identification. The tooth contours are matched in the spatial domain, while the contours of dental works are matched in both spatial and frequency domains. To reduce alignment error, a point-reliability method as well as an outlier detection and pruning method are designed for contour matching. With these techniques, promising experimental results were obtained. However, these 2D radiograph based approaches still suffer from several limitations. (1) X-ray radiographs are usually noisy and blurred, which makes the tooth segmentation and contour extraction time-consuming and inaccurate. Chen and Jain [3] reported that 14 out of 25 subjects in their database could not be identified. Furthermore, human intervention is often required in preprocessing. (2) Some important features are distorted in radiographs. For example, the dental arch which is considered to be unique among individuals [18] is usually distorted in 2D radiographs. (3) 2D radiographs are less informative compared to 3D records since 2D images are projections of 3D teeth. 3D dental feature details such as the ridges and grooves on each tooth are lost in 2D images.

To overcome the inherent limitations of 2D based methods, 3D dental identification approaches were proposed based on matching 3D dental records [8,9]. In [9] for example, salient points were automatically detected which are used to register the PM model to the AM model, and the iterative closest point (ICP) [19] was adopted to compute the matching scores. It achieved 80% Rank-1 recognition rate on 60 PM to 200 AM subjects, and took 45 min on average to identify one subject from 200 subjects (on a PC with a Core 2 Dual CPU 2.5 GHz and 4 GB RAM). We can see that there is still much room for improving the accuracy and speed.

In this work, we propose an efficient 3D dental identification approach via learning based feature point extraction and a novel shape descriptor called the Signed Feature Histogram (SFH). An overview of our approach is shown in Fig. 1. In the offline part, we establish a small training dataset which is a subset of the AM database and label a series of keypoints at the desired positions. The local surface of every labeled keypoint is then described by the SFH which can be efficiently computed. The labeled keypoints along with the descriptors are used to train a Random Forest (RF) model, based on which the keypoints on both AM and PM models can be accurately detected. In the online part, the given PM model is efficiently identified by matching the SFHs to those of AM models followed by ICP refinement. The main contributions of this work are:

- A machine learning based keypoint detection method is used to accurately detect a sparse set of keypoints on the dental models.
- A novel shape descriptor is proposed to describe the local shape which can be easily and efficiently computed.
- A highly efficient dental identification approach is presented by matching the descriptors of the keypoints followed by ICP refinement.
- Comparative experiments are conducted on a public dataset to evaluate the SFH performance with results showing that SFH outperforms the state-of-the-art descriptors.
- Comparative experiments are conducted on 3 different PM dental datasets containing complete, incomplete and single tooth respectively. Both high accuracy and efficiency are achieved.

The remainder of this paper is organized as follows. In Section 2, we describe the data acquisition and preprocessing steps. In Section 3, we introduce a machine learning approach for keypoint detection and the Signed Feature Histogram descriptor for representing the local information of the keypoints. An efficient dental identification method is presented in Section 4. In Section 5, comparison experiments are conducted to testify the performance of the proposed descriptor and the identification method. The computational time statistics are also presented. Finally, we conclude our work in Section 6.

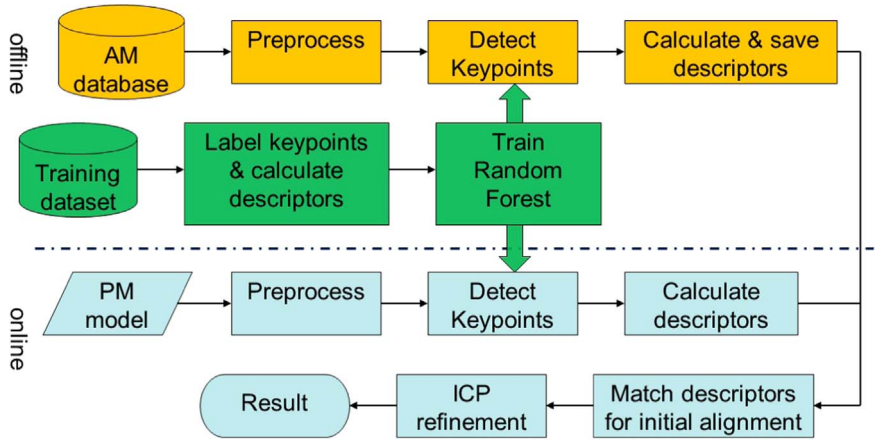

Fig. 1. Block diagram of the proposed 3D dental identification approach.

2. Data acquisition and preprocessing

In this section, we describe the antemortem (AM) and postmortem (PM) dataset acquisition and 3 critical preprocessing steps including decimation, segmentation, and remeshing.

2.1. Data acquisition

Antemortem (AM) models: Plaster samples are taken from 200 subjects whose ages range from 12 to 35 years. These plaster samples are then scanned using the Minolta VIVID 900 Surface Laser Scanner with the spatial scanning resolution of 0.2 mm.

Postmortem (PM) models: Postmortem (PM) models are taken independently by another investigator in the following year using the same laser scanner. This time, 20 subjects are selected from the 200 subjects sampled previously. To verify the effectiveness of our method, we construct three PM datasets: complete, incomplete and single tooth datasets. Details can be found in Section 5.

2.2. Preprocessing

The raw data is noisy and requires between 14 MB and 40 MB of storage per mouth. We perform 3-step preprocessing on the AM models and PM models including decimation, segmentation, and remeshing.

Decimation: Since the scanning is performed under high resolution, the resulting models have 340,000–400,000 triangle faces. We reduce the models to 10% of the original size for higher computational speed. The simplification method proposed in [20] is employed as it can output a high quality approximation. Fig. 2 (b) shows an example of the decimated model.

Segmentation: In the second step, we perform automatic segmentation to remove the bottom part of the digitized plaster where tooth information does not exist. The Principal Component Analysis (PCA)-plane passing through the centroid of the model is used to cut the model into two parts (Fig. 2(c)).

Remeshing: Remeshing [21] is another important preprocessing step which makes the model vertices regularly distributed (e.g. all edges have approximately the same lengths). Comparing Fig. 2 (d) and (e), it is clear that the vertices are more regularly distributed after remeshing.

3. Learning based keypoint detection

A keypoint, also referred to as interest point or feature point, plays a crucial role in many computer vision applications such as retrieval [22], object registration [23], object recognition [24,25], and face recognition [26]. In this section, we introduce a robust 3D dental keypoint detection scheme. The following criteria are well-recognized for good keypoint detection methods.

Repeatability: The keypoints should be highly repeatable, that is, the keypoints are detected consistently across different instances of the same object.

Descriptiveness: There should be enough information around keypoints so that descriptive features can be extracted.

Small quantity: Fewer but representative keypoints are preferred. A small number of keypoints can significantly reduce computational complexity and improve matching accuracy.

In existing works [27–29], keypoints are usually detected based on the metric of curvature or saliency, resulting in a large number of redundant keypoints. To achieve efficiency, the detected keypoints should not only be of high repeatability and high descriptiveness but should also be small in number. To this end, we introduce a learning based keypoint detection scheme which comprises mainly three steps: (1) we label a very small number of representative dental keypoints on the training datasets. (2) For each labeled keypoint we build a novel shape descriptor to represent the local surface. (3) The descriptors of the labeled keypoints are fed into the Random Forest to train a model, based on which the keypoints can then be predicted. We detail these steps in the following subsections.

3.1. Keypoint labeling

We classify the teeth into 4 categories: incisor, canine, molar, and premolar. The center of the masticating surface of each tooth is labeled as the keypoint (Fig. 3). Such labeling has the advantages that useful information is gathered on the masticating surface, and each model can be represented by a very small number of keypoints (one keypoint per tooth). 280 keypoints have been labeled on 40 dental models. Each keypoint is assigned a class label (incisor, canine, premolar, or molar), and the local surface patch will be described by descriptors which are used to train a classifier.

3.2. An novel shape descriptor

To train the classifier, we need to construct shape descriptors

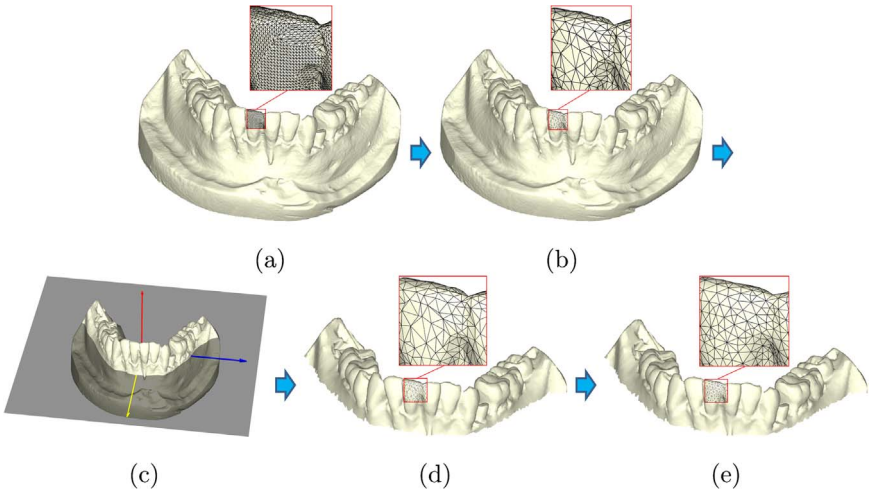

Fig. 2. Preprocessing procedure: (a) original dental model; (b) dental model after decimation; (c) principal component analysis (PCA) plane construction; (d) the upper part is kept as segmentation result; (e) final dental model after remeshing.

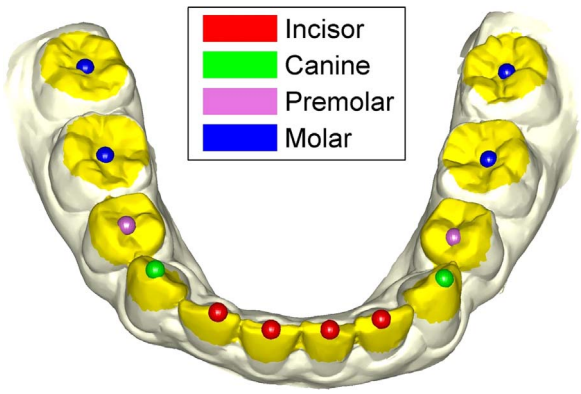

Fig. 3. For each of training model, the desired keypoints on incisor, canine, molar, and premolar are manually labeled whose local surface patches will be described by descriptors and fed into a classifier for training.

for the keypoints to describe the local characteristics so that the classifier knows the types of vertices that are keypoints. There are many available descriptors ranging from simple single-value based descriptors like curvature [27] and saliency map [28,29] to more complex signature or histogram based descriptors such as spin images [30], SHOT [31], RoPS [32]. Creusot et al. [33] detected facial keypoints using both simple and complex descriptors. However, they reported that complex descriptors could decrease identification efficiency.

In this work, we propose a novel shape descriptor named the Signed Feature Histogram (SFH) that is highly discriminative and can also be efficiently computed. The proposed descriptor is an extension of our previous work [34]. The major improvements lie in three aspects. First, SFH is a 3D descriptor encoding more information. Second, SFH is more discriminative as two out of the three dimensions are associated with signs. Third, a highly reliable and repeatable Local Reference Axis is used to make the descriptor more stable.

3.2.1. Local Reference Axis

The Local Reference Axis (LRA) or Local Reference Frame (LRF) is crucial for robust feature description. The descriptor could be more stable and discriminative if a transformation invariant LRF or LRA is provided. Some early works used the single normal vector as the LRA [30,35,36] which lack descriptiveness. Recent works [31,37,32] emphasized the importance of the LRF.

However, the main problem of the LRF is the instability of the x- and y-axes. In [37], for example, the x-axis is the direction from the keypoint to the point with largest angle between its normal and the z-axis, which is unstable in the presence of noise. Recent popular methods construct the LRF by finding the major direction of the scatter vectors [31,32]. The stability is largely improved while the sign ambiguity of the x and y axes still exists. Another disadvantage of the LRF is that more computational time is required compared to LRA. This problem becomes more obvious when a large number of descriptors need to be built. Based on these considerations, we use a highly repeatable and reliable LRA instead of the LRF to build the descriptor, since the former can be efficiently computed without the sign ambiguity problem of the x and y axes.

Given a keypoint p on the surface and a support radius r, we construct the LRA as the weighted sum of normals of all the vertices within the local support, that is

$$\mathrm{LRA} = \sum_{i=1}^{N} w_i n_i \tag{1}$$

where N is the number of vertices within local support, and w_i is computed as

$$w_i = (r - |p - p_i|) / \sum_{i=1}^{N} (r - |p - p_i|).$$

Here, p_i is a neighboring vertex within the local support. w_i measures the distance from the keypoint to the neighboring p_i. We assign a greater weight to a neighboring vertex which is close to p, and assign a smaller weight to a vertex which is far away from p.

3.2.2. Signed feature histogram

With the Local Reference Axis (LRA), we now are able to construct the shape descriptor called Signed Feature Histogram (SFH for short), which is an extension of our previous work [34]. This time, the new descriptor is extended into 3D and more signed features are encoded. The SFH is constructed as follows.

For a keypoint p on the surface (Fig. 4, left), the local surface within radius r is defined as S_p which is mapped into the 3D domain by using the following equation:

$$S_p \rightarrow (\alpha, \beta, \theta) = (|(x - p) \times \mathrm{LRA}_p|, D_1 \cdot (x - p) \cdot \mathrm{LRA}_p, D_2 \cdot \theta_x), \tag{2}$$

where LRA_p is the Local Reference Axis (LRA) computed at p, LRA_x is the LRA of a neighboring vertex x in the local support. θ_x represents the included angle between LRA_p and LRA_x which is computed by $\arccos(\mathrm{LRA}_p \cdot \mathrm{LRA}_x)$. D_1 is the sign of the perpendicular distance from x to the tangent plane determined by

$$D_1 = \begin{cases} +1, & \mathrm{LRA}_p \cdot (x - p) > 0 \\ -1, & \text{otherwise} \end{cases}$$

and D_2 is the sign of the angle between LRA_p and LRA_x determined by

$$D_2 = \begin{cases} +1, & \mathrm{LRA}_p \cdot (x - p) < \mathrm{LRA}_x \cdot (x - p) \\ -1, & \text{otherwise} \end{cases}$$

When x is above the tangent plane D_1 is assigned $+1$, otherwise it is assigned -1. For D_2, it is assigned $+1$ when LRA_x point towards LRA_p, otherwise it is assigned -1.

After mapping the vertices within S_p into the 3D domain, we uniformly divide the range of the three dimensions into k bins. The SFH is constructed by allocating the vertices of S_p into different

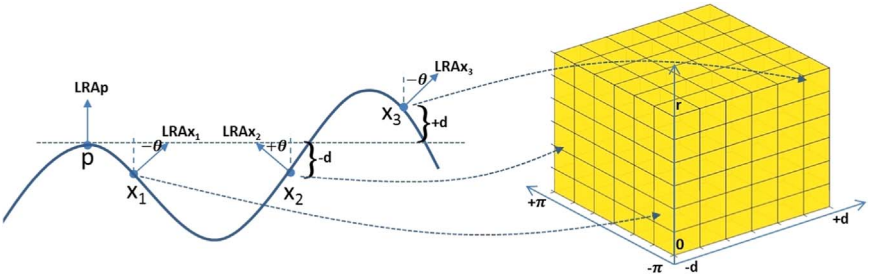

Fig. 4. Signed Feature Histogram (SFH) construction.

bins according to their 3D values. The value of a particular bin is the number of vertices that fall into this bin. The final SFH is shown on the right of Fig. 4 where the axis ranges from 0 to r indicates the perpendicular distance to the LRA_p, the axis ranges from $-r$ to $+r$ represents the perpendicular distance from x to the tangent plane, and the axis ranges from $-\pi$ to $+\pi$ represents the signed angle. We build SFHs for all the keypoints in the training set, which will then be fed into a classifier for learning. The keypoints in our case are from four classes: incisor, canine, premolar and molar. Therefore, a multiclass classification technique is required. Popular classifiers such as neural networks [38], naive Bayes [39], extensions of support vector machines [40,41] and Random Forest [42] are applicable to this problem. In this study, we use the Random Forest for our task because it is a natural multiclass classifier having the appealing advantages of high accuracy, robustness, and high computational efficiency in both training and classification.

3.3. Keypoint detection via Random Forest

The proposed descriptor Signed Feature Histogram (SFH) represents the local surface of any vertex in a canonical form, thus allowing us to train a classifier which can then be used to predict the desired keypoints. Here, we employ the Random Forest [42] for this task due to its competitive accuracy and high efficiency. Learning based keypoint detection commonly involves two stages: offline training and online prediction.

3.3.1. Training

In the training stage, 20 complete dental models are collected. We annotate the keypoints on each model at the desired positions, as shown in Fig. 3, as well as the class labels (incisor, canine, premolar or molar). The keypoints are represented by SFHs which encode the local surface characteristics in a canonical form. Finally, we obtain a training dataset comprising 280 keypoints associated with SFHs and class labels denoted as $\{D_i = (S_i, c_i)\}$, where S_i is the SFH descriptor and c_i is the class label.

The Random Forest trains each tree independently following a random sampling scheme in order to increase the robustness and avoid overfitting on the training data. For keypoint detection, a subset of training samples for each class is randomly selected. Then, the tree is trained in a recursive way, where, for each node of the tree, a subset of features out of S_i is chosen randomly based on which, the best split is calculated. The process is repeated for the left and right child nodes. The tree is fully grown without pruning until a stopping criterion is met [42]. After training, a non-leaf node is labeled with a split function $f_\Phi(S_i) \in (0, 1)$ which optimally separates the training samples, while each leaf of the tree is labeled with a probability distribution over the classes.

3.3.2. Prediction

The trained Random Forest classifier can be used for dental keypoint prediction. As an ensemble classifier, it consists of a collection of decision trees where each individual tree gives a probability distribution. The final prediction result is determined by averaging the probability distributions given by each tree. Fig. 5 illustrates how an input vertex is predicted by the Random Forest. The vertex on a dental model is first described by the Signed Feature Histogram (SFH) which goes down each decision tree of Random Forest. The class membership probability $P(c)$ for the current input is generated at the leaf node of the tree. In Fig. 5, the vertex (blue point) to be predicted is close to the desired molar keypoint position. Thus, the probability to the molar class (blue bar) is much higher, indicating that it is more likely to be a molar keypoint. By examining the average probability distribution over all the trees, we can classify the input as a keypoint when certain probability value of the average distribution is high enough.

An example of dental keypoint detection is shown in Fig. 6. For efficiency, we set the tooth centered part as the Region of Interest (ROI) and discard the points close to the model boundary. SFHs are computed for the points in ROI and fed into the Random Forest for prediction. Since there are four classes (incisors, canines, premolars or molars), we have four probability maps as shown in the second row of Fig. 6. The vertex with a high probability (red) is more likely to be a member of that class, and thus should be selected as a keypoint. From the four maps, we see that most of the

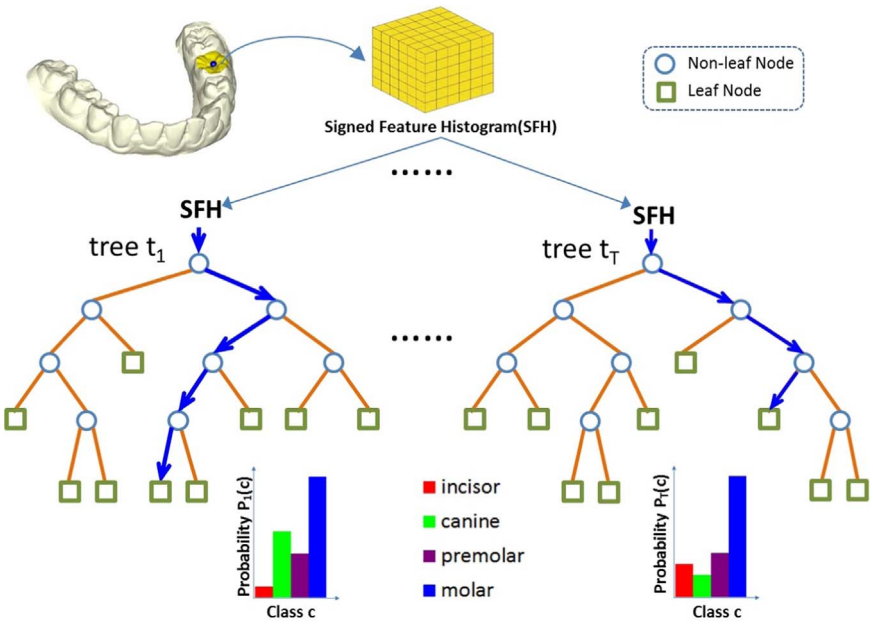

Fig. 5. Dental keypoint prediction via Random Forest: the vertex to be predicted is described by SFH which traverses each tree of the Random Forest from the root node to the corresponding leaf node. The path direction (blue path) is routed by the split function at the non-leaf node. The leaf node gives a probability distribution over classes indicating the membership probability that the input sample belongs to a specific class. The final prediction result is determined by analyzing the probability distribution over classes computed by averaging the distributions of the leaf nodes reached in every tree. The taller blue bar in this example means that the input sample is more likely to be a molar keypoint. (For interpretation of the references to color in this figure caption, the reader is referred to the web version of this paper.)

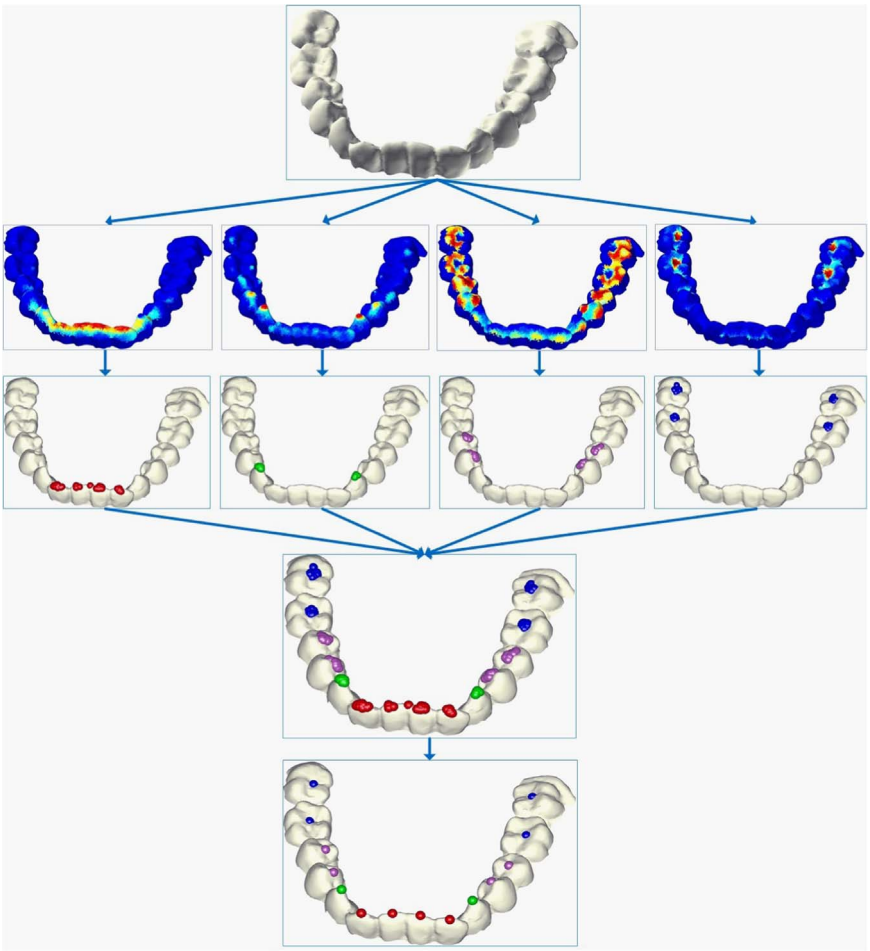

Fig. 6. Given a dental model (top row), the Region of Interest (ROI) is defined as the tooth centered region by setting the region close to the boundary as non-ROI. SFHs are computed for the points of ROI which are fed into the Random Forest for prediction. The probability maps (second row) of the 4 teeth classes are generated using Random Forest. From left to right, the maps for incisor, canine, premolar and molar are shown with range from 0 (blue) to 1 (red). The vertices with higher probability value (e.g. above threshold value t) are considered as potential keypoints (third row). The fourth row shows the aggregation of the potential keypoints of all the four classes. The local maxima are detected as final keypoints (bottom row). (For interpretation of the references to color in this figure caption, the reader is referred to the web version of this paper.)

high probability points are aggregated at the desired keypoint positions. For the premolar map, however, some points on the molar also possess high probabilities. This indicates that the local characteristics of these points are similar to those of the premolar. To filter them out, we set a threshold value $t=0.95$ and select vertices with probabilities above t as keypoints (third row of Fig. 6). Such a selection still produces multiple keypoints at each desired position as nearby vertices possess similar characteristics. To further suppress the non-max probability keypoints, only the local maxima are considered as final keypoints (bottom row of Fig. 6).

4. Dental identification

The identification procedure has been shown in Fig. 1. This procedure consists two parts. In the offline part, every model in the AM database is pre-processed and the keypoints are detected using the method described above. Local shape descriptors (SFHs) are then constructed for all the keypoints. In the online part, the same processes are implemented for a given PM model. However, the non-maximum probability keypoints are not suppressed for the AM models to make sure that each keypoint of a PM model has a corresponding keypoint on the AM model.

To identify a given PM model, we need to compare it to each of the AM models and choose the most similar one as the correct match. Given a pair of AM and PM models (denoted as $M1$ and $M2$) to be compared, we denote their keypoints as $K1$ and $K2$ respectively ($|K2| < |K1|$). To measure their similarity the following steps are conducted. First, we build a list containing L potential correspondences for each keypoint of $K2$ from $K1$ ($L \ll |K1|$) by checking the similarities of the SFHs. That is, for each element of $K2$, the l_2 distances between its SFH and the SFHs of all the elements of $K1$ are calculated and sorted in an ascending order. The first L elements from $K1$ are chosen as the potential correspondences for the current keypoint of $K2$. In the second step, we randomly select three different keypoints from $K2$ whose potential corresponding keypoints are selected from their potential lists. This results in $L_* L_* L$ different 3-to-3 combinations. For each possible combination, we compute the rigid transformation matrix to transform the PM model to the AM model. The mean square error (MSE) between the two models after transformation is used to estimate the transformation accuracy. In most cases, the above procedure can output an accurate transformation based on which we can finally obtain the final similarity between these two models. However, to enhance the robustness we iterate this procedure N times and choose the one with minimum MSE as the best initial alignment which is then refined by the iterative closest point (ICP) [19] algorithm. The ICP result serves as the final measurement of the similarity of the given pair. The matching procedure is

summarized in Algorithm 1, with $N=100$, $L=5$.

Algorithm 1. Matching a pair of dental models.

Input:
Antemortem (AM) and Postmortem (PM) Models: $M1$, $M2$;
Keypoints sets of $M1$ and $M2$: $K1$, $K2$ with $K2 \subseteq K1$;
SFHs at the keypoints of $M1$ and $M2$: $S1$, $S2$;

$LIST_{|K2|\times L} \leftarrow 0$
for each keypoint in $K2$ **do**
  find L potential correspondences from $K1$ by checking the similarities of the SFHs, and stored as potential list;
end for
$n \leftarrow 0$; $minDist \leftarrow Inf$; $T_{best} \leftarrow \phi$;
repeat
  Randomly select 3 keypoints P from $K2$; For each of their potential correspondences Q in $LIST_{|K2|\times L}$
  if $COMPATIBLE(P, Q)$ **then**
    Compute the rigid transformation matrix T and do rigid transformation; Compute the Mean Square Error (MSE) d between the two models after transformation;
    if $d \le minDist$ **then**
      $minDist \leftarrow d$; $T_{best} \leftarrow T$;
    end if
  end if
  $n \leftarrow n + 1$;
until $n > N$
Do rigid transformation with T_{best} and run ICP algorithm for refinement; compute the MSE S between the two models after ICP refinement.

Output
The similarity score: S

Algorithm 2. Check the compatibility of two groups of keypoints.

procedure COMPATIBLE(P, Q)
if $|P| \neq |Q|$ **then**
  return false
else
  $n \leftarrow |Q|$;
  $flag \leftarrow$ **true**;
  for $i = 1 \rightarrow n - 1$ **do**
    for $j = 2 \rightarrow n$ **do**
      $d1 \leftarrow \| P(i) - P(j) \|$
      $d2 \leftarrow \| Q(i) - Q(j) \|$
      $thr \leftarrow 0.2_{*} \min(d1, d2)$
      $s \leftarrow abs(d1 - d2)$;
      if $s > thr$ **then**
        flag $\leftarrow$ **false**
      end if
    end for
  end for
end if
return flag;
end procedure

It is worth noting that it is unwise to apply ICP directly for identification because without good initial alignment, ICP is computationally expensive and easily gets stuck in local minima. The initial alignment is established robustly and efficiently in our algorithm because of the descriptive descriptor and the learning keypoints.

5. Experimental results

In this section, we evaluate the performances of the Signed Feature Histogram (SFH) and dental identification method. For the SFH, the discriminative power is analyzed on a public dataset and comparisons are made with another 3 state-of-the-art descriptors. The performance of dental identification method is investigated on three different PM datasets comprising complete, incomplete and single tooth PM models, respectively. We also test the running time in each experiment. The codes are written in Matlab and run on a laptop with Pentium Dual-Core CPU 2.5 GHz and 4 G RAM without any program optimization.

5.1. Performance of the SFH

The choice of descriptor is crucial for both keypoint detection and matching. We use SFH for these tasks because it is easy to compute and highly discriminative. To verify its appealing properties, we compare SFH with another 3 state-of-the-art descriptors including Spin Image [30], SHOT [31], and RoPS [32] on a public dataset.

5.1.1. Dataset and evaluation methodology

The SFH is tested on the Bologna Dataset [31] comprising 6 models and 45 scenes. The 45 scenes are built up by randomly rotating and translating different subsets of the 6 models to create clutter. The transformation matrices are saved, from which we can easily obtain the ground truth correspondences between the vertices of each model and their instances in the scene. Noise occurs in image acquisition and will thus lead to dissimilarity between the PM and AM dental models of the same subject. To evaluate the robustness of our algorithm, three levels of Gaussian noise corresponding to 10%, 30% and 50% of the average mesh resolution (mr for short) are added to the scene data. A scene example and its noisy versions are shown in Fig. 7.

For each model, 1000 feature points are randomly selected. The corresponding feature points are extracted from the scenes. All the feature points are described by descriptors. The scene feature points are matched against all the model feature points by matching the descriptors. If the Euclidean distance between descriptors for a particular pair of feature points is below a set threshold, we call this pair a match. A correct positive indicates a match where the two feature points correspond to the same physical location, while a false positive is a match where two feature points are from different physical locations. We employ recall (3) vs. 1-precision (4) (RP) curve to evaluate the performance which is generated by varying the threshold.

$$\text{recall} = \frac{\text{number of correct positives}}{\text{total number of positives}} \tag{3}$$

$$1 - \text{precision} = \frac{\text{number of false positives}}{\text{total number of matches (correct or false)}} \tag{4}$$

The top left corner of the RP curve is the point where the feature obtains both high recall and precision which represents a perfect test.

5.1.2. SFH parameters

The support radius r and number of bins L are two parameters that affect the performance of SFH. The support radius controls the amount of local region encoded into the SFH descriptor. With a large r, SFH can capture more local information and thus become more informative and descriptive. However, the sensitivity to occlusion and clutter is also increased. On the contrary, a small r is

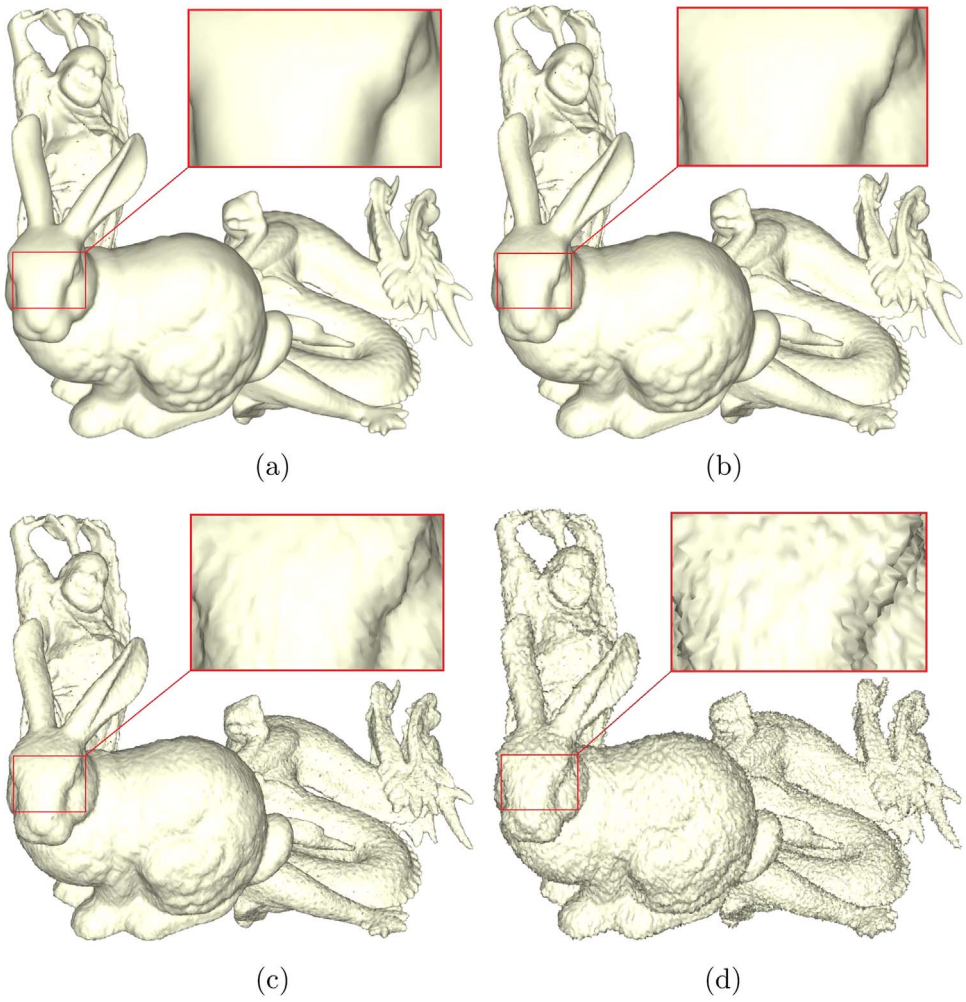

Fig. 7. A scene example (a) and its noisy versions with Gaussian noise of 10% mr (b), 30% mr (c), and 50% mr (d) are shown. The zoom-in pictures (red rectangles) show the noise levels in detail. (For interpretation of the references to color in this figure caption, the reader is referred to the web version of this paper.)

more robust to occlusion and clutter at the cost of low descriptiveness. Thus, r can be set depending on the practical application and actual data distribution. For the descriptor evaluation, the radius r is set as 10 times mr, which is considered as a tradeoff on the Bologna Dataset.

Another important parameter is the number of bins L computed as $k \times k \times k$. Here, k is the number of divisions along each SFH axis. A SFH with larger L has more discrimination power, as the distribution of the local surface is described more precisely. However, very fine bin quantization does not mean high recall and precision because the descriptor will become sparse and sensitive to noise. The performance of the SFH is accessed with respect to different numbers of bins where k is set as 4, 6, 8, 10, and 12. The experimental results are shown in Fig. 8. In general, the performance is improved by increasing the number of bins. Significant improvement is observed by varying k from 4 to 6. This indicates that the local surface is not fully described by the SFH with k smaller than 6. However, for k between 6 and 12, the variances between the RP curves are not distinct because SFH with $k=6$ well describes the local surface and there is no much room for improvement. For the scenes with 0.5 mr noise (Fig. 8(d)), large k can even decrease the SFH performance. We see that the SFH with $k=12$ performs slightly worse than that with $k=10$.

5.1.3. Comparisons with other descriptors

The SFH is compared with Spin Image [30], SHOT [31], and RoPS [32]. The parameter values for the descriptors to be compared are listed in Table 1. For a fair comparison, the same support radius (10 mr) is set for all the descriptors. The rest of the parameters are tuned to achieve the optimal performance in terms of the RP Curve. Again, to test the robustness to noise, the experiments are conducted on both noisy free scenes and the scenes with different levels of noise. The comparison results are shown in Fig. 9.

Overall, SFH outperforms the other 3 descriptors on both noise free and noisy scene data. For the noise free scenes (Fig. 9 (a)), the results of SFH and RoPS are almost equal with SFH performing slightly better than RoPS followed by SHOT and Spin Image. With increasing noise (Fig. 9(b)–(d)), SFH is still the best with much higher recall and precision than others. For the scenes with noise levels of 10% mr and 30% mr, SHOT works better than RoPS while RoPS performs better than SHOT for the scenes with 50% mr noise. This is consistent with the conjecture made by [32] that RoPS is more competent than SHOT under high level of noise. As the noise level increases, the performance of Spin Image deteriorates sharply. This is due to the fact that the Spin Image as a 2D descriptor is less informative than SHOT and SFH. Our SFH outperforms other descriptors in all the cases. The robustness of our SFH descriptor can be explained by two facts. First, signed feature encoding makes SFH much more discriminative, so that SFH can robustly find the correct correspondences for both noise free and noisy scenes. Second, the LRA is more stable than LRF. LRA is computed by weighting the neighboring mesh faces and examining the normal vector direction, while the LRF comprises three axes where

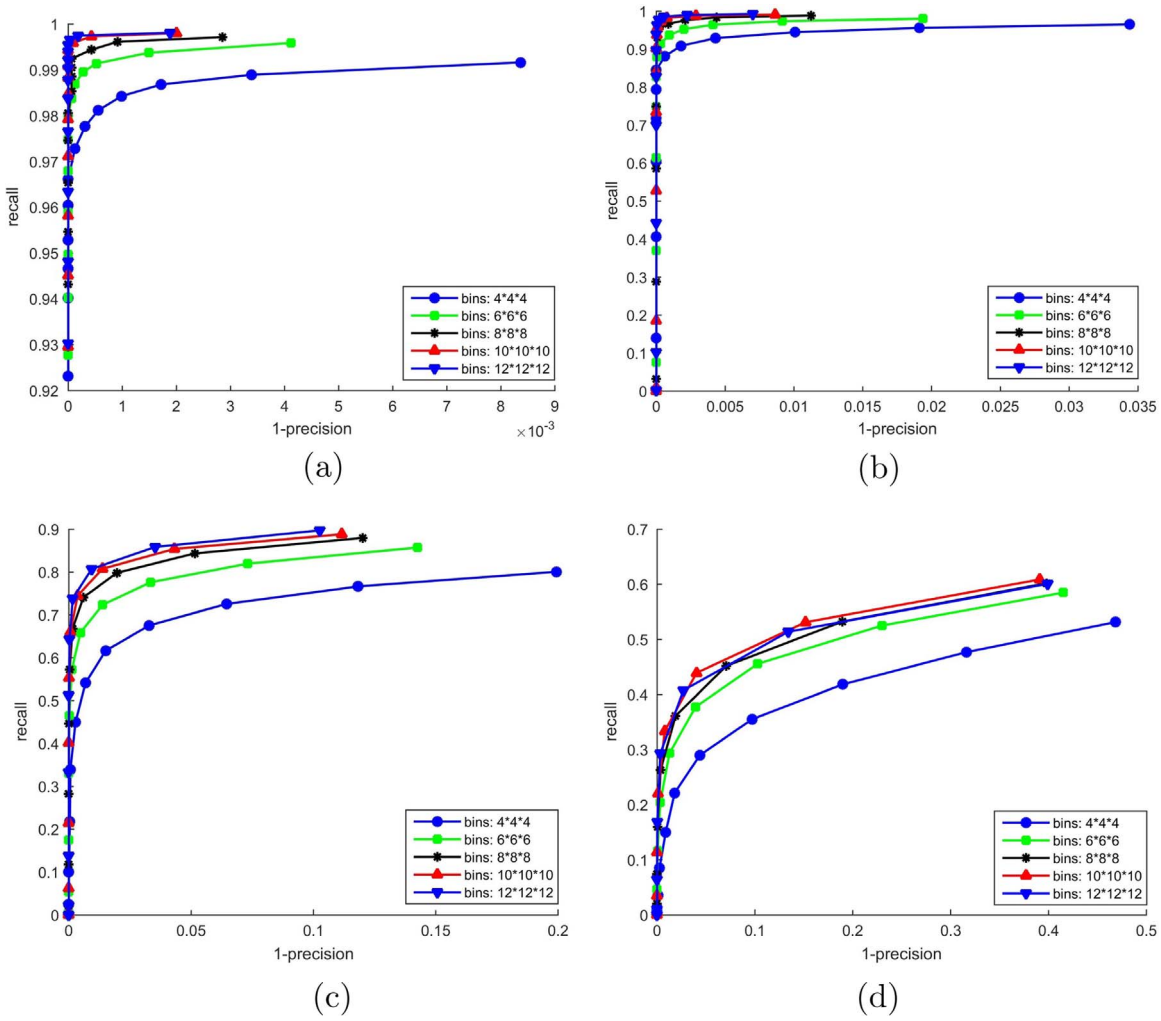

Fig. 8. Recall vs. 1-Precision curves for testing the performance with respect to different numbers of bins on matching the scenes with 0% (a), 10% (b), 30% (c), and 50% (d) mr levels of noise respectively.

Table 1
Descriptor parameters.

Name	Radius (mr)	Dimensionality	Length
Spin image	10	15×15	225
SHOT	10	$8 \times 2 \times 2 \times 10$	320
RoPS	10	$3 \times 3 \times 3 \times 5$	135
SFH-6	10	$6 \times 6 \times 6$	216
SFH-8	10	$8 \times 8 \times 8$	512

the x and y are unstable and suffer from the sign ambiguity problem.

From the comparisons, we note that the performances of SFH-6 and SFH-8 are quite similar with SFH-8 slightly better than SFH-6. However, the SFH-8 length is two times longer than SFH-6, and longer length can decrease the matching efficiency. Thus, in the subsequent experiments, we choose SFH-6 as it is discriminative enough for our application.

5.1.4. Timing

Besides the discriminative power of SFH, the computational time is another reason that we choose SFH. We run the four descriptors 1000 times and the computational time is shown in Table 2. We can see that SFH runs faster than SHOT and RoPS but lightly slower than Spin Image. This is another important aspect that needs to be considered since in reality the descriptor usually runs tens of thousands of times.

5.2. Performance of dental identification

The performance of the proposed dental identification method is evaluated on 3 datasets including complete, incomplete, and single tooth PM models respectively.

5.2.1. Parameter setting

Before starting the experiments, we need to set several parameters. The number of bins of SFH descriptor is set as $6 \times 6 \times 6$ as stated in Section 5.1.2. The local support radius r is set as 6 which ensures sufficient local region coverage as well as resistance to clutter. For the ICP algorithm which is used to refine the initial matching, we set the maximum number of iterations N_{iter} and the minimum error change err as 200 and 0.0001 respectively since such settings can generate accurate matching scores without losing the efficiency.

5.2.2. Performance of complete dental identification

In this experiment, we investigate the performance of our proposed identification method on 20 complete PM dental models. The quantitative identification results are shown in Table 3, from which we see that our method outperforms [9] by achieving 100% Rank-1 accuracy for all 20 PM models. Such an excellent

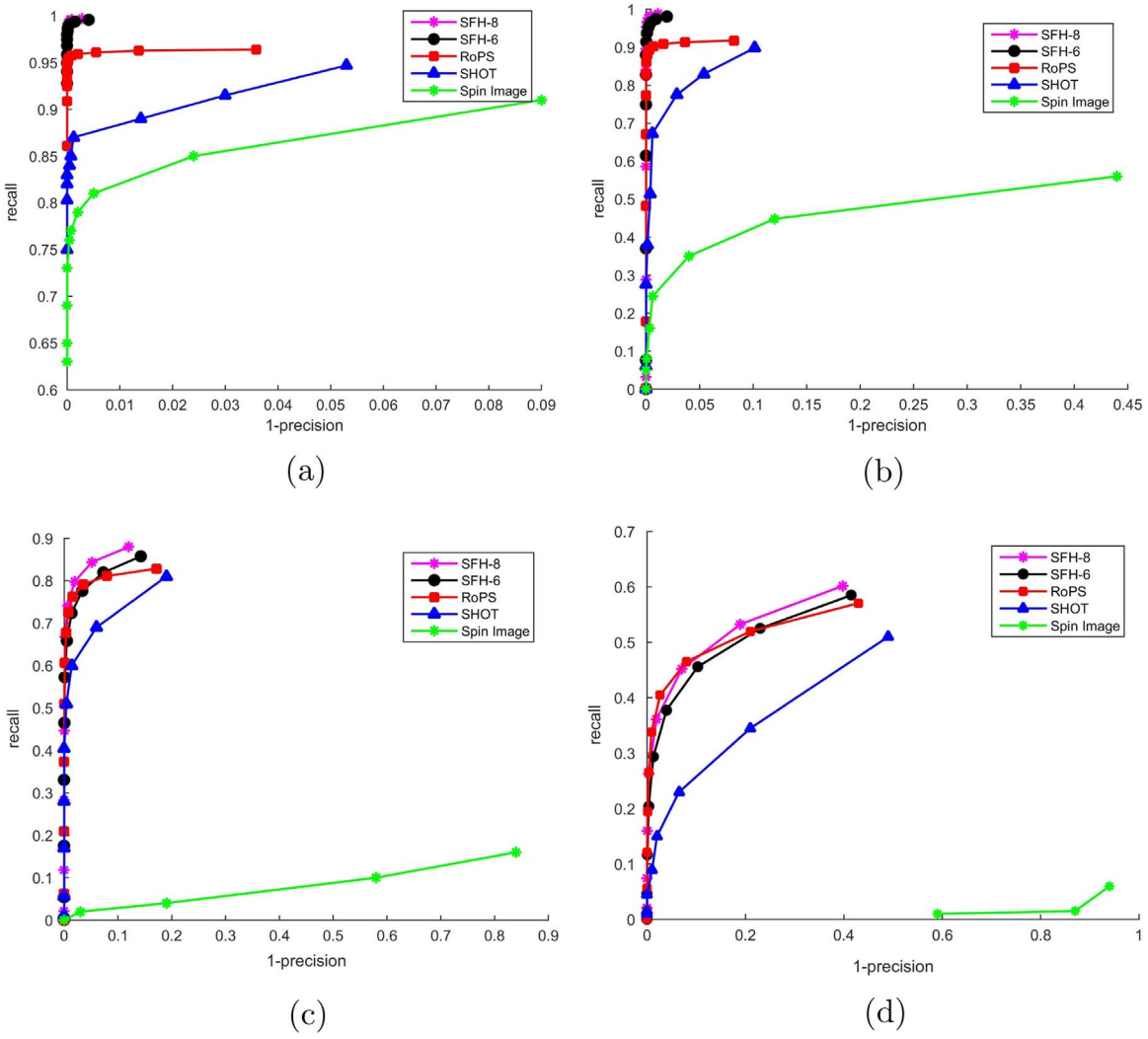

Fig. 9. Recall vs. 1-Precision curves of different methods for matching scenes with 0% (a), 10% (b), 30% (c), and 50% (d) mr levels of noise respectively.

Table 2
Time cost for building 1000 descriptors.

Spin image	SHOT	RoPS	SFH
4.1	7.5	12.8	4.33

Table 3
Accuracy of complete dental identification.

PM 1–10	1	2	3	4	5	6	7	8	9	10
This work	1	1	1	1	1	1	1	1	1	1
Zhong et al. [9]	1	1	1	1	1	1	1	1	1	1
PM 11–20	11	12	13	14	15	16	17	18	19	20
This work	1	1	1	1	1	1	1	1	1	1
Zhong et al. [9]	1	1	1	1	2	1	1	1	1	1

result is mainly due to the robust keypoint detection and the effective matching algorithm we have proposed. On the one hand, fewer representative keypoints can largely reduce the failure cases since a larger number of keypoints can produce more possible matches and thus increase the failure chance. On the other hand, learning based keypoint detection can produce keypoints precisely located at the desired positions so that the correspondences between the keypoints of the PM and AM models can be found accurately. Based on the correspondences, the subsequent initial alignment can be accomplished and the ICP refinement can robustly converge to the global minimum and generate an accurate matching score. By analyzing the keypoint correspondences, we see that the failure cases usually occur when the initial 3-to-3 correspondences are wrongly established. We select 6 pairs of dental models (PM 1, 2, 4, 11, 13, 15) and plot the initial 3-to-3 correspondences found by the two methods in Fig. 10. By analyzing the keypoint correspondences, we see that the failure case occurs when the initial 3-to-3 correspondences are wrongly established. Our method can always find the correct 3-to-3 correspondences, while [9] fails in the PM15 which causes incorrect identification.

5.2.3. *Performance of incomplete dental identification*

Due to violence or accident, the PM model may become incomplete, e.g., for the same person the PM model can only partially match the AM model (see Fig. 11). In such cases, an identification method that can handle partial matching would be required. Most 2D methods relying on tooth contours assume no missing teeth in the images and the performance may decrease when this assumption is violated. In the 3D method [9], feature matching and the ICP algorithm are employed to match incomplete dental models. Despite the promising results, PM models with too many missing teeth cannot be well recognized.

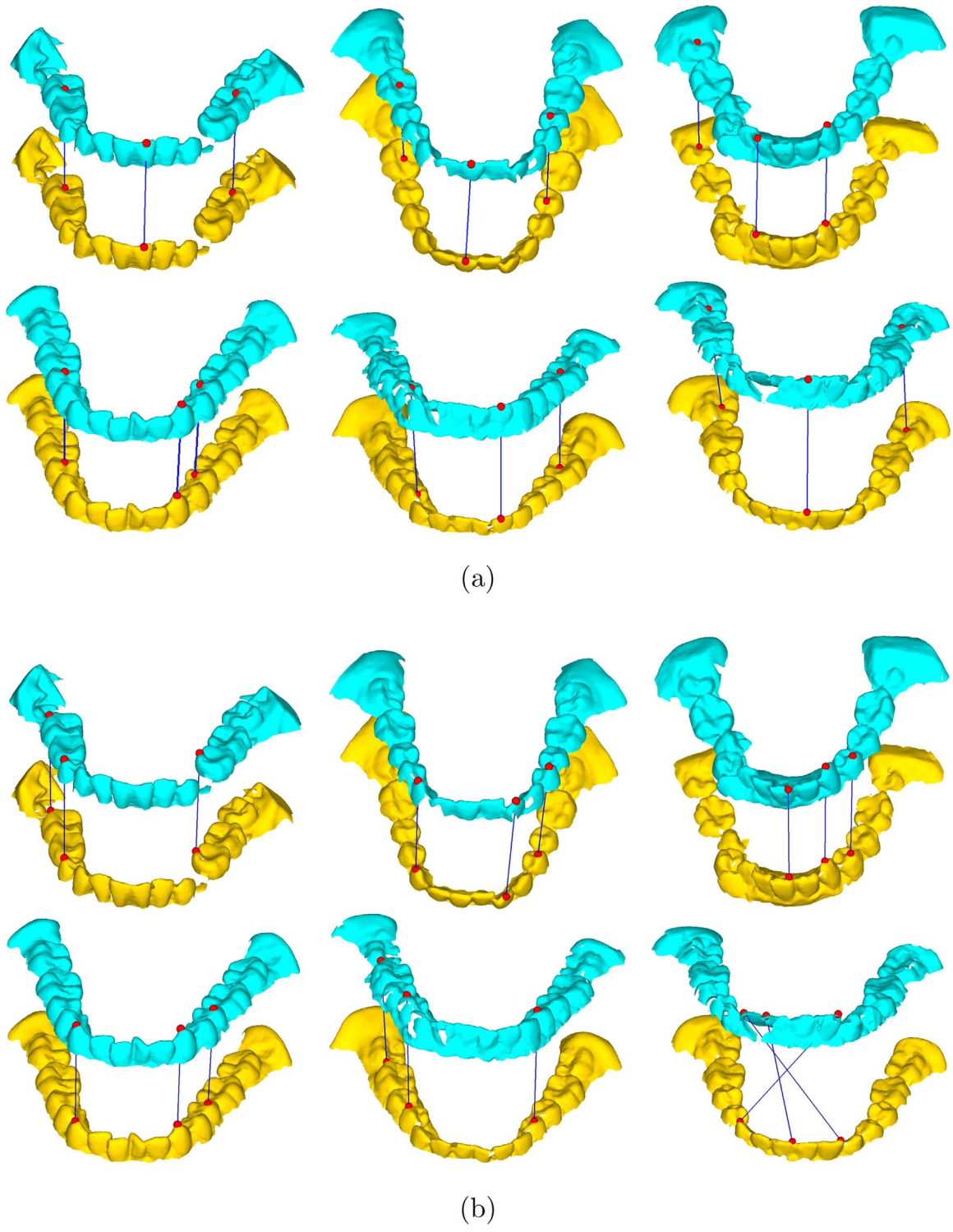

Fig. 10. The correspondences (blue lines) found by our method (a) and Zhong et al. [9] (b) between the keypoints of the complete PM (cyan) and AM (golden) models. (For interpretation of the references to color in this figure caption, the reader is referred to the web version of this paper.)

In this experiment the performance of the proposed method is tested on 20 incomplete PM models. The identification results are reported in Table 4. All the PM models are correctly identified with 100% Rank-1 accuracy. Compared with [9] which matches feature points based on a single value descriptor, our descriptor SFH is more informative and discriminative. Based on the powerful SFH and the effective matching scheme, the correspondences between the keypoints of AM and PM models can be robustly established even for a partial model. The matching examples are shown in Fig. 11. We select the same 6 model pairs (PM 1,2,4,11,13,15) as in matching complete dental models and plot the correspondences between the dental keypoints found by our method and [9]. For some models with very large missing parts like PM4 and PM15, our algorithm is still able to accurately find the correspondences. Again, we find that the PM models with incorrect correspondences happen to be the failure cases in Table 4. Thus, we can conclude that the robust initial keypoint matching is crucial to the identification result, and our method is able to achieve the goal.

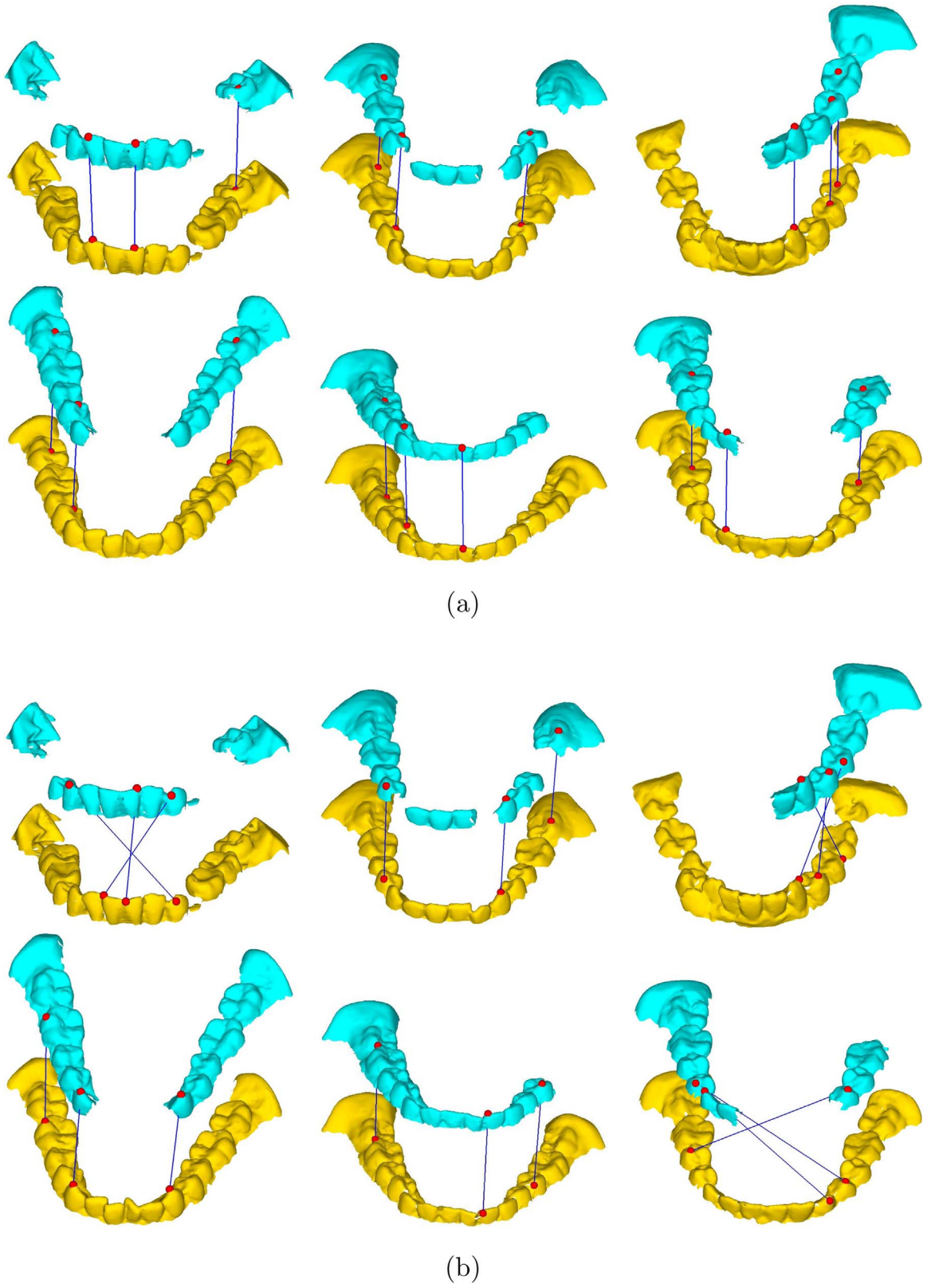

Fig. 11. The correspondences (blue lines) found by our method (a) and Zhong et al. [9] (b) between the keypoints of the incomplete PM (cyan) models and AM (golden) models. (For interpretation of the references to color in this figure caption, the reader is referred to the web version of this paper.)

It also should be noted that in this experiment the retained order and relative placement of the teeth are also important to achieve the high recognition results on incomplete dental identification. For an incomplete model with distinct change of tooth order and relative placement, our method cannot work well since matching the whole PM model against the AM models cannot produce a correct score. In this case, a method which is able to identify single teeth is required.

Table 4
Accuracy of incomplete dental identification.

PM 1–10	1	2	3	4	5	6	7	8	9	10
This work	1	1	1	1	1	1	1	1	1	1
Zhong et al. [9]	3	1	1	4	1	3	1	1	1	1
PM 11–20	11	12	13	14	15	16	17	18	19	20
This work	1	1	1	1	1	1	1	1	1	1
Zhong et al. [9]	1	1	1	1	2	1	1	1	1	1

5.2.4. Performance of single tooth identification

Under certain severe conditions such as fire or collision, the jawbone may be broken into pieces, and only scattered teeth are available. In this case, single tooth identification becomes imperative. This is a more challenging task since one tooth contains much less information compared to the complete and incomplete dental models. To the best of our knowledge, there is no previous research on this topic.

The PM single tooth dataset is created by manually clipping the complete PM models into single tooth pieces. For each of the 20 complete PM models, we pick four teeth from the clipped pieces with one tooth per type (incisor, canine, premolar and molar). Finally, we obtain a test dataset containing 80 single tooth models. Each tooth is matched against all the AM models. There are 200 AM models in the database with each containing 14 to 16 teeth. Thus, each PM tooth needs to be matched against approximately 3000 teeth. Traditional methods cannot handle such a challenging identification problem because very little information is contained in one tooth and there are too many possible matches in the database.

Thanks to the robust keypoint detection and discriminative descriptor, our method is able to identify the single tooth by matching the descriptors and Local Reference Frames (LRFs) of the keypoints. We cannot directly apply our method (see Section 4) for this task since only one keypoint is detected on the single tooth and the initial alignment that transforms the given tooth to the potential tooth requires at least three corresponding keypoints to compute the transformation matrix. To solve this problem, we superimpose three additional points at each keypoint using the endpoints of the three axes of LRF. The method of [32], which is shown to be highly stable and repeatable, is employed to compute the LRF. Equipped with LRF, the matching problem is transformed into matching the LRFs. Fig. 12 shows the matching procedure. Given a single tooth as input, we detect the keypoint which is associated with the LRF and the descriptor SFH. To determine its identity, the input LRF is matched against the LRFs of all the keypoints in the database. For each matching, we determine the optimal orientation between the LRFs such that the input tooth can fit well with the AM tooth. The final score is obtained by the ICP refinement.

The Cumulative Match Characteristic (CMC) is employed to illustrate the identification performance. As shown in Fig. 13, the horizontal axis represents the rank of retrieved subjects while the vertical axis indicates the identification accuracy. We can see that 73.75% Rank-1 accuracy is achieved. We also present some of the matching examples in Fig. 14, from which we see that most PM single tooth models are matched correctly while some failures occur on incisor models as indicated by the circles. This is mainly because an incisor contains too few distinctive features, and thus cannot be differentiated from other incisors even with a discriminative descriptor.

5.2.5. Timing

The mean computational time of each step of the dental identification method on the three types of PM dental models is shown in Table 5. The running time for preprocessing, SFH computation, and keypoint detection replies on the number of vertices involved. Thus, it takes more time on complete PM dataset than other two types of datasets for these three steps. Take the complete PM dataset for example. The preprocessing step takes 1 s on average. The number of vertices after preprocessing ranges from 9200 to 13,600. It takes around 14 s to construct SFHs for every vertex based on which keypoints are predicted. Since the Random Forest has been trained offline, the online keypoints prediction can be finished within 1.0 s. The matching step, which is the most time consuming part, involves searching the database and matching AM models one by one via initial alignment and ICP refinement. In our approach, this step can be done within 300 s. This is 9 times faster than the 3D method [9] which takes 45 min on average, and about 80 times faster than the 2D method which takes 7 h for the identification of one subject. It is also noted that the single tooth identification takes more time on matching step, since a single tooth is matched against approximately 3000 teeth in the AM database.

We also analyze the time for matching step with regard to the database size (Fig. 15). For the three categories, it takes more time with the AM database size increases. In the future, we can accelerate the process by adopting other method to filter out large number of irrelevant models. For instance, we can extract and match the dental arches first to efficiently filter out many AM models.

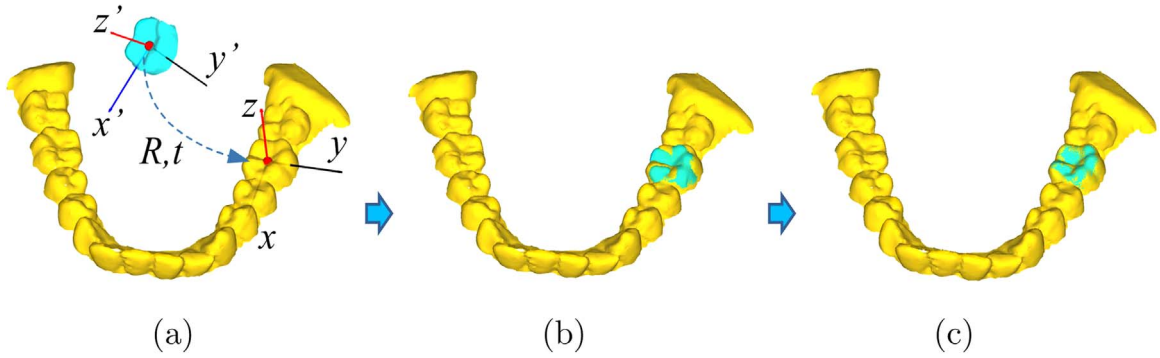

Fig. 12. Single tooth matching procedure: (a) Local Reference Frames (LRFs) are created at the keypoints of PM single tooth model and the tooth of AM model using the method proposed in [32]. Here, the x', y' and z' form the LRF of the PM tooth, while the LRF of the desired tooth is constructed by x, y and z. The rigid transformation comprising rotation R and translation t is computed with regard to the LRFs. (b) Then, the initial alignment can be achieved by transforming the single tooth model. (c) The final matching score is calculated by refining the initial alignment via the Iterative Closest Point algorithm [19].

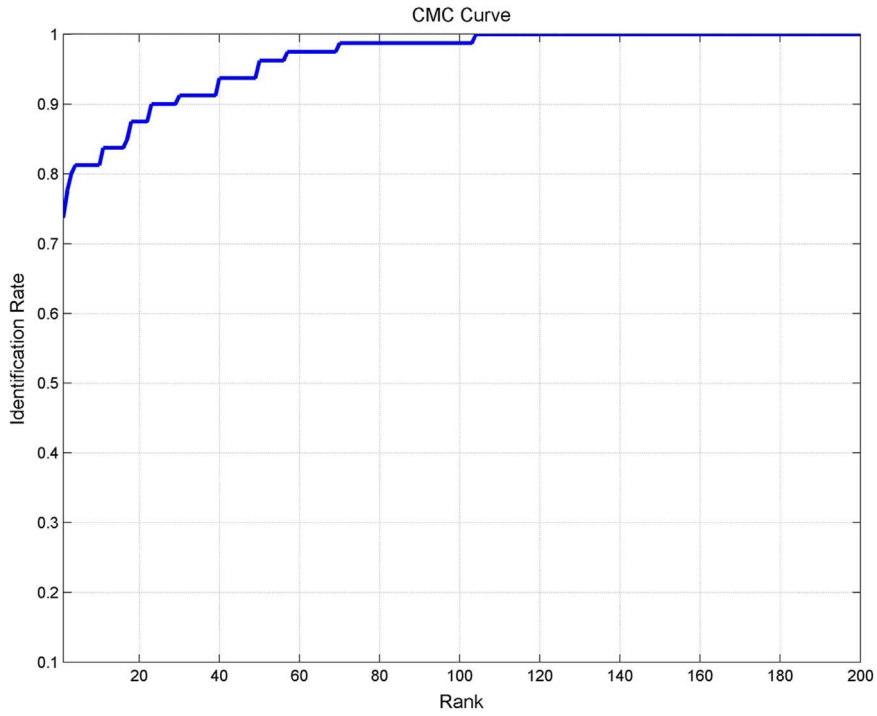

Fig. 13. CMC curve of single tooth identification.

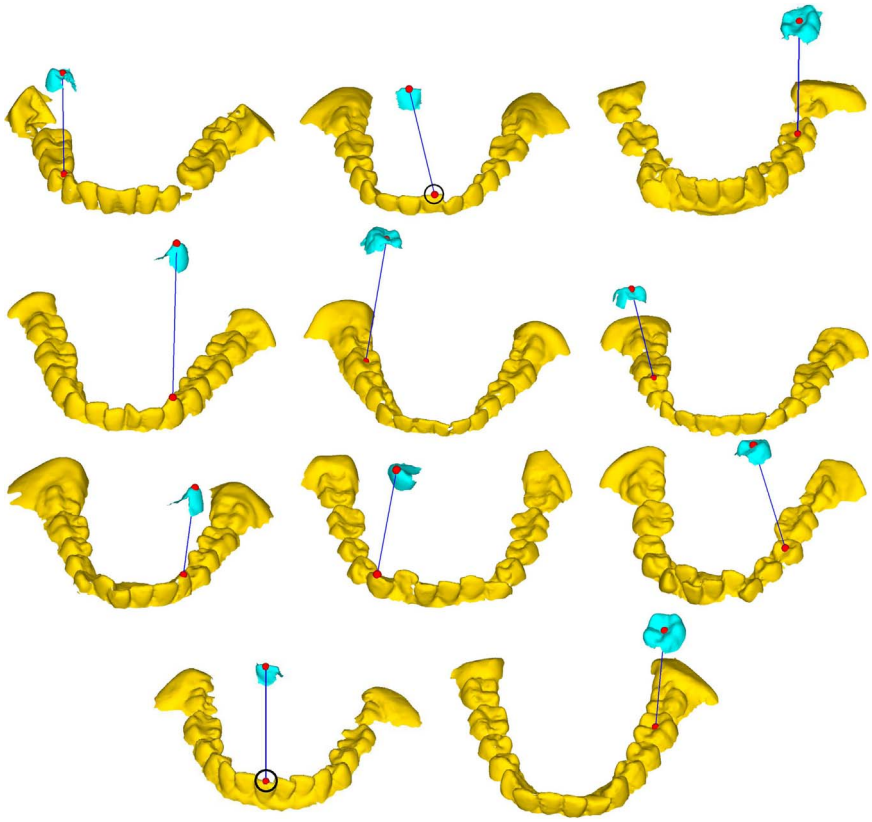

Fig. 14. The correspondences (blue lines) found by our method between the keypoints of the single tooth PM (cyan) models and AM (golden) models. (For interpretation of the references to color in this figure caption, the reader is referred to the web version of this paper.)

6. Conclusions

In this work, we introduce an efficient dental identification method through learning based keypoint detection and a novel shape descriptor named Signed Feature Histogram (SFH). A Random Forest (RF) model is trained by pre-labeled keypoints and associated SFHs. With the RF model, the keypoints on both AM and PM models are accurately detected. Finally, based on the detected keypoints and the associated SFHs, an efficient identification approach is proposed. To verify the proposed method, we conduct

Table 5
Dental identification time statistics of each step of our proposed approach.

Model type	Preprocess	SFH Comp.	Keypoint Det.	Matching	Total
Complete	1.2	13.4	0.7	267.8	284.1
Incomplete	0.7	9.2	0.5	178.2	181.2
Single	0.1	1.2	0.1	307.5	310.5

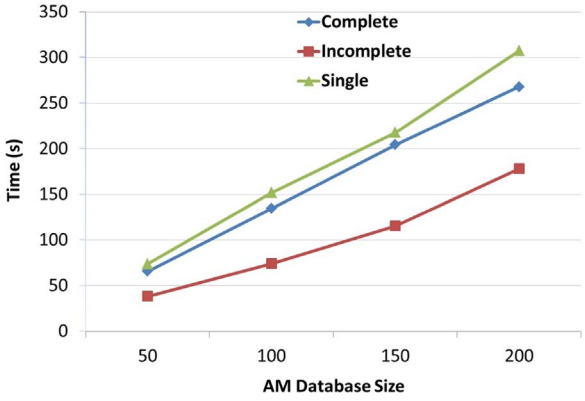

Fig. 15. Computational time with regard to the database size.

experiments on three different datasets containing complete, incomplete and single tooth models respectively. Experimental results show that our method achieves superior performance in both accuracy and efficiency. We obtain 100% Rank-1 accuracy on both complete and incomplete datasets and 73.75% Rank-1 accuracy on the single tooth dataset. To test the performance of our method for PM models having large rotations with respect to the AM models, we also perform an experiment on PM models with various rotations. Experimental results confirm that the proposed method is rotation and translation invariant. And the running time is only 300 s on average to identify one complete PM dental model from 200 AM models. This is about 80 times faster than many 2D methods which usually take several hours to identify one subject.

The success of our method mainly lies in three aspects. First, we use a learning scheme to accurately detect the keypoints on the dental models. These keypoints, which are in very small size, can largely accelerate the matching process and decrease the matching error. Second, the proposed local shape descriptor SFH is informative and discriminative which can be fast computed. Base on the SFHs, the correspondences can always be correctly established. Third, the matching algorithm proposed in Section 4 can robustly identify the PM dental model in a very efficient manner.

References

[1] A.K. Jain, H. Chen, S. Minut, Dental biometrics: human identification using dental radiographs, in: Audio-and Video-Based Biometric Person Authentication, 2003, pp. 429–437.
[2] A.K. Jain, H. Chen, Matching of dental x-ray images for human identification, Pattern Recognit. 37 (7) (2004) 1519–1532.
[3] H. Chen, A.K. Jain, Dental biometrics: alignment and matching of dental radiographs, IEEE Trans. Pattern Anal. Mach. Intell. 8 (2005) 1319–1326.
[4] J. Zhou, M. Abdel-Mottaleb, A content-based system for human identification based on bitewing dental x-ray images, Pattern Recognit. 38 (11) (2005) 2132–2142.
[5] O. Nomir, M. Abdel-Mottaleb, A system for human identification from x-ray dental radiographs, Pattern Recognit. 38 (8) (2005) 1295–1305.
[6] O. Nomir, M. Abdel-Mottaleb, Human identification from dental x-ray images based on the shape and appearance of the teeth, IEEE Trans. Inf. Forensics Secur. 2 (2) (2007) 188–197.
[7] P.-L. Lin, Y.-H. Lai, P.-W. Huang, Dental biometrics: human identification based on teeth and dental works in bitewing radiographs, Pattern Recognit. 45 (3) (2012) 934–946.
[8] X. Zhong, D. Yu, T. Sim, Y. San Wong, H.-l. Cheng, Towards automated pose invariant 3d dental biometrics, in: International Joint Conference on Biometrics, 2011, pp. 1–7.
[9] X. Zhong, D. Yu, Y.S. Wong, T. Sim, W.F. Lu, K.W.C. Foong, H.-L. Cheng, 3d dental biometrics: alignment and matching of dental casts for human identification, Comput. Ind. 64 (9) (2013) 1355–1370.
[10] P. Lin, Y. Lai, P. Huang, An effective classification and numbering system for dental bitewing radiographs using teeth region and contour information, Pattern Recognit. 43 (4) (2010) 1380–1392.
[11] P. OShaughnessy, More than half of victims idd, New York Daily News 11.
[12] P. Thepgumpanat, Thai tsunami forensic centre produces first ids, Reuters, 18, ⟨http://www alertnet.org⟩.
[13] New scientist news – dental records beat DNA in tsunami IDs.
[14] G. Fahmy, H. Chen, O. Nomir, R. Howell, M. Abdel-Mottaleb, A.K. Jain, H. H. Ammar, J. Zhou, D. Nassar, E. Haj-Said, Toward an automated dental identification system, J. Electron. Imaging 14 (4) (2005) 1–13.
[15] O. Sweet, et al., Interpol dvi best-practice standards—an overview, Forensic Sci. Int. 201 (1) (2010) 18–21.
[16] O. Nomir, M. Abdel-Mottaleb, Hierarchical contour matching for dental x-ray radiographs, Pattern Recognit. 41 (1) (2008) 130–138.
[17] O. Nomir, M. Abdel-Mottaleb, Fusion of matching algorithms for human identification using dental x-ray radiographs, IEEE Trans. Inf. Forensics Secur. 3 (2) (2008) 223–233.
[18] J.A. Kieser, V. Bernal, J. Neil Waddell, S. Raju, The uniqueness of the human anterior dentition: a geometric morphometric analysis, J. Forensic Sci. 52 (3) (2007) 671–677.
[19] P.J. Besl, N.D. McKay, A method for registration of 3-d shapes, IEEE Trans. Pattern Anal. Mach. Intell. 14 (2) (1992) 239–256.
[20] M. Garland, P.S. Heckbert, Surface simplification using quadric error metrics, in: Proceedings of the 24th Annual Conference on Computer Graphics and Interactive Techniques, 1997, pp. 209–216.
[21] S. Boyé, G. Guennebaud, C. Schlick, Least squares subdivision surfaces, Comput. Graph. Forum vol. 29 (2010) 2021–2028.
[22] R. Ohbuchi, K. Osada, T. Furuya, T. Banno, Salient local visual features for shape-based 3d model retrieval, in: IEEE International Conference on Shape Modeling and Applications, 2008, SMI 2008, 2008, pp. 93–102.
[23] N. Gelfand, N. J. Mitra, L. J. Guibas, H. Pottmann, Robust global registration, in: Symposium on Geometry Processing, vol. 2, 2005, p. 5.
[24] Y. Guo, M. Bennamoun, F. Sohel, M. Lu, J. Wan, 3d object recognition in cluttered scenes with local surface features: a survey, IEEE Trans. Pattern Anal. Mach. Intell. 36 (11) (2014) 2270–2287.
[25] O.J. Woodford, M.-T. Pham, A. Maki, F. Perbet, B. Stenger, Demisting the hough transform for 3d shape recognition and registration, Int. J. Comput. Vis. 106 (3) (2014) 332–341.
[26] A.S. Mian, M. Bennamoun, R. Owens, Keypoint detection and local feature matching for textured 3d face recognition, Int. J. Comput. Vis. 79 (1) (2008) 1–12.
[27] T. Gatzke, C. Grimm, M. Garland, S. Zelinka, Curvature maps for local shape comparison, in: International Conference on Shape Modeling and Applications, 2005, pp. 244–253.
[28] C.H. Lee, A. Varshney, D. W. Jacobs, Mesh saliency, in: ACM Transactions on Graphics, vol. 24, 2005, pp. 659–666.
[29] U. Castellani, M. Cristani, S. Fantoni, V. Murino, Sparse points matching by combining 3d mesh saliency with statistical descriptors, Comput. Graph. Forum vol. 27 (2008) 643–652.
[30] A.E. Johnson, M. Hebert, Using spin images for efficient object recognition in cluttered 3d scenes, IEEE Trans. Pattern Anal. Mach. Intell. 21 (5) (1999) 433–449.
[31] F. Tombari, S. Salti, L. Di Stefano, Unique signatures of histograms for local surface description, in: European Conference on Computer Vision, 2010, pp. 356–369.
[32] Y. Guo, F. Sohel, M. Bennamoun, M. Lu, J. Wan, Rotational projection statistics for 3d local surface description and object recognition, Int. J. Comput. Vis. 105 (1) (2013) 63–86.
[33] C. Creusot, N. Pears, J. Austin, A machine-learning approach to keypoint detection and landmarking on 3d meshes, Int. J. Comput. Vis. 102 (1–3) (2013) 146–179.
[34] Z. Zhang, S.H. Ong, K.W.C. Foong, Improved spin images for 3d surface matching using signed angles, in: IEEE International Conference on Image Processing, 2012, pp. 537–540.
[35] A. Frome, D. Huber, R. Kolluri, T. Bülow, J. Malik, Recognizing objects in range data using regional point descriptors, in: European Conference on Computer Vision, 2004, pp. 224–237.
[36] H. Chen, B. Bhanu, 3d free-form object recognition in range images using local surface patches, Pattern Recognit. Lett. 28 (10) (2007) 1252–1262.
[37] A. Petrelli, L. Di Stefano, On the repeatability of the local reference frame for partial shape matching, in: IEEE International Conference on Computer Vision, 2011, pp. 2244–2251.
[38] C.M. Bishop, Neural Networks for Pattern Recognition, Oxford University Press, Oxford, 1995.
[39] I. Rish, An empirical study of the naive Bayes classifier, in: IJCAI 2001 Workshop on Empirical Methods in Artificial Intelligence, vol. 3, 2001, pp. 41–46.
[40] J. Weston, C. Watkins, Multi-class Support Vector Machines, Technical Report, 1998.
[41] E.J. Bredensteiner, K.P. Bennett, Multicategory classification by support vector machines, Comput. Optim. (1999) 53–79.
[42] L. Breiman, Random forests, Mach. Learn. 45 (1) (2001) 5–32.

Zhiyuan Zhang received the Bachelor degree from the Yanshan University in 2005 and the Master degree from the Harbin Institute of Technology in 2008. He has worked as a research assistant at the department of computing of Hong Kong Polytechnic University from 2008 to 2009. He received his Ph.D. degree from the National University of Singapore in 2015. He is currently a staff researcher at the Lenovo Group Limited. His research interests include computer vision, computer graphics, geometric processing, and biometrics.

Sim Heng Ong received the B.E.(Hons.) degree from the University of Western Australia, Perth, WA, Australia, and the Ph.D. degree from the University of Sydney, Sydney, NSW, Australia. He is currently an Associate Professor in the Department of Electrical Engineering and the Department of Bioengineering, National University of Singapore, Singapore. His current research interests include computer vision and biomedical image processing. He has authored or coauthored more than 250 papers published in international journals and conference proceedings.

Xin Zhong is currently working as a scientist in Institite of High Performance Computing (IHPC) at Agency for Science, Technology and Research (A*STAR). She received her Ph.D. degree in Mechanical Engineering Department, National University of Singapore. Her research interests include 3D dental biometrics, data mining, medical image processing and 3D measurement technology.

Kelvin W.C. Foong is a specialist dental surgeon. He graduated from the National University of Singapore with the Dental degree in 1988, and received speciality training at The University of Adelaide, Australia, from 1992 to 1994, and the Ph.D. degree in 2005, having studied the topic of 3D surface imaging of cleft palate deformity in infants. He is currently an Associate Professor in the Faculty of Dentistry, National University of Singapore. He also holds the appointment of Senior Consultant in Orthodontics at the National University Hospital. His current research interests include the application of 3-D image processing and visualization techniques for the development of accurate, patient-specific virtual models of the teeth, face, and head. He works in close collaboration with research partners in the fields of Vision Engineering and Image Processing to develop virtual models of the face and teeth.